Normal ovarian surface epithelial label-retaining cells exhibit stem/progenitor cell characteristics

Paul P. Szotek*, Henry L. Chang*, Kristen Brennand†, Akihiro Fujino*, Rafael Pieretti-Vanmarcke*, Cristina Lo Celso‡, David Dombkowski§, Frederic Preffer§, Kenneth S. Cohen‡, Jose Teixeira¶, and Patricia K. Donahoe*‖

*Pediatric Surgical Research Laboratories, Massachusetts General Hospital and Harvard Medical School, Boston, MA 02114; §Flow Cytometry Laboratory, Department of Pathology and Center for Regenerative Medicine, Massachusetts General Hospital, Boston, MA 02114; †Howard Hughes Medical Institute, Harvard Stem Cell Institute and the Department of Molecular and Cellular Biology, Harvard University, Cambridge, MA 02139; ¶Vincent Center for Reproductive Biology, Massachusetts General Hospital, Boston, MA 02114; and ‡Center for Regenerative Medicine, Harvard Stem Cell Institute, Massachusetts General Hospital, Boston, MA 02114

Contributed by Patricia K. Donahoe, May 27, 2008 (sent for review May 5, 2008)

Ovulation induces cyclic rupture and regenerative repair of the ovarian coelomic epithelium. This process of repeated disruption and repair accompanied by complex remodeling typifies a somatic stem/progenitor cell-mediated process. Using BrdU incorporation and doxycycline inducible histone2B-green fluorescent protein pulse–chase techniques, we identify a label-retaining cell population in the coelomic epithelium of the adult mouse ovary as candidate somatic stem/progenitor cells. The identified population exhibits quiescence with asymmetric label retention, functional response to estrous cycling *in vivo* by proliferation, enhanced growth characteristics by *in vitro* colony formation, and cytoprotective mechanisms by enrichment for the side population. Together, these characteristics identify the label-retaining cell population as a candidate for the putative somatic stem/progenitor cells of the coelomic epithelium of the mouse ovary.

somatic stem cells | ovarian coelomic epithelium

The ovarian coelomic epithelium covers the ovary as a layer of squamous or cuboidal cells. Folliculogenesis in the adult ovary is characterized by extensive architectural remodeling that culminates in disruption of the coelomic epithelium and extrusion of the ovum at ovulation (1, 2). After disruption, a series of molecular events initiates and executes repair of the epithelial wound (3, 4). The cyclic pattern of repeated disruption and repair with complex remodeling associated with ovulation leads one to intuit the existence of a population of somatic stem/progenitor cells that would be responsible for these processes. Additionally, previous studies of the coelomic epithelium (CE) have implicated cyclic re-epithelialization as the source of accrued mutations leading to ovarian cancer (5).

Somatic stem cells are a subset of normal tissue cells that, through asymmetric division, have the ability to self renew and produce lineage committed daughter cells responsible for tissue regeneration and repair (6, 7). Injury-responsive stem cells and their niches have been described in a variety of tissues, such as skin and hair follicle (6, 8, 9), mammary gland (10, 11), and intestine (6, 12). In some tissues, slow-cycling somatic stem cells were initially identified by their ability to retain label for long periods of time, whereas asymmetrically derived lineage committed daughter cells dilute out label during rapid proliferation and terminal differentiation (9, 13–18). These studies, as well as the recent identification of label-retaining cells (LRCs) in the uterine endometrial stroma and myometrium (19), used BrdU, 3H-Thymidine, or histone2B-green fluorescent protein (H2B-GFP) labeling to identify candidate somatic stem cells. The functional capacity of the identified candidate cells could subsequently be confirmed evaluating *in vivo* and *in vitro* behavior. Characterization of these cells could then lead to the discovery of tissue-specific surface markers.

Additionally, somatic and cancer stem cells from various tissues have been identified by their ability to efflux Hoechst 33342 dye through ATP-binding-cassette transporters, such as Abcg2/Bcrp1 (11, 20–27), including our recent identification of these "side population" (SP) cells as potential tumor-initiating cells in ovarian cancer (28). It has been postulated that this chemical-effluxing capability contributes to the cytopreservation necessary for the longevity attributed to stem/progenitor cells (29). Thus, label retention and Hoechst dye efflux are two distinct methods that can be used to identify candidate somatic stem cells.

Using BrdU and H2B-GFP transgenic mice as models, we have identified a population of long term LRCs in the coelomic ovarian surface epithelium that were studied further for functional characteristics as defined *in vivo* by functional proliferative response to the estrous cycle and *in vitro* by robust colony formation and enrichment of GFP cells in the SP.

Results

Identification of BrdU and H2B-GFP Label Retaining Cells in the Coelomic Epithelium. We used pulse–chase labeling with BrdU and tetracycline-regulated (doxycycline responsive) H2B-GFP fusion protein in female mice to identify a slow-cycling LRC population in the mouse ovary [supporting information (SI) Fig. S1*A*]. Rosa26-rtTA; tetO-H2B-GFP (H2B-GFP) mice were generated and provided by Brennand and colleagues (30). The H2B-GFP animals were pulsed during the embryonic period (E0-P42) or as an adult (6 wk–10 wk) to determine which one gave the better ovarian staining (see Fig. S1*B*) and found the adult pulsed animals resulted in better labeling. BrdU animals were pulsed as adults (6 wk–7 wk).

To validate the ability of H2B-GFP mice to identify somatic stem cells, flow cytometry was used to compare bone marrow GFP LRCs to the hematopoietic stem cell phenotype $Lin^{-}cKit^{+}Sca\text{-}1^{+}$ (31, 32). Analysis of H2B-GFP whole bone marrow indicated that $Lin^{-}cKit^{+}Sca\text{-}1^{+}$ cells preferentially retain the H2B-GFP label (Fig. 1, Fig. S2). These findings confirm that the H2B-GFP model can identify somatic stem cells.

Ovarian H2B-GFP and BrdU labeling was evaluated by immunofluorescence. PBS injected (no BrdU) and naive (no doxycycline) H2B-GFP mice were used as negative controls (not shown). Significant variability in whole ovary pulse labeling was observed by computerized image analysis of all three experiments performed in this study (see Fig. 1*A*, Fig. S3*A*) (embryonic pulse H2B-GFP = 26.0 ± 2.5%, adult pulse H2B-GFP = 82.5 ± 7.9%, adult pulse BrdU = 46.9 ± 8.9%). Despite this initial pulse labeling variation,

Author contributions: P.P.S., H.L.C., K.B., J.T., and P.K.D. designed research; P.P.S., H.L.C., K.B., A.F., R.P.-V., C.L.C., D.D., F.P., K.S.C., and J.T. performed research; P.P.S., H.L.C., K.B., J.T., and P.K.D. analyzed data; and P.P.S., H.L.C., and P.K.D. wrote the paper.

The authors declare no conflict of interest.

‖To whom correspondence should be addressed at: Pediatric Surgical Research Laboratories, Massachusetts General Hospital, 185 Cambridge Street, CPZN 6.100, Boston, MA 02114. E-mail: pdonahoe@partners.org.

This article contains supporting information online at www.pnas.org/cgi/content/full/0805012105/DCSupplemental.

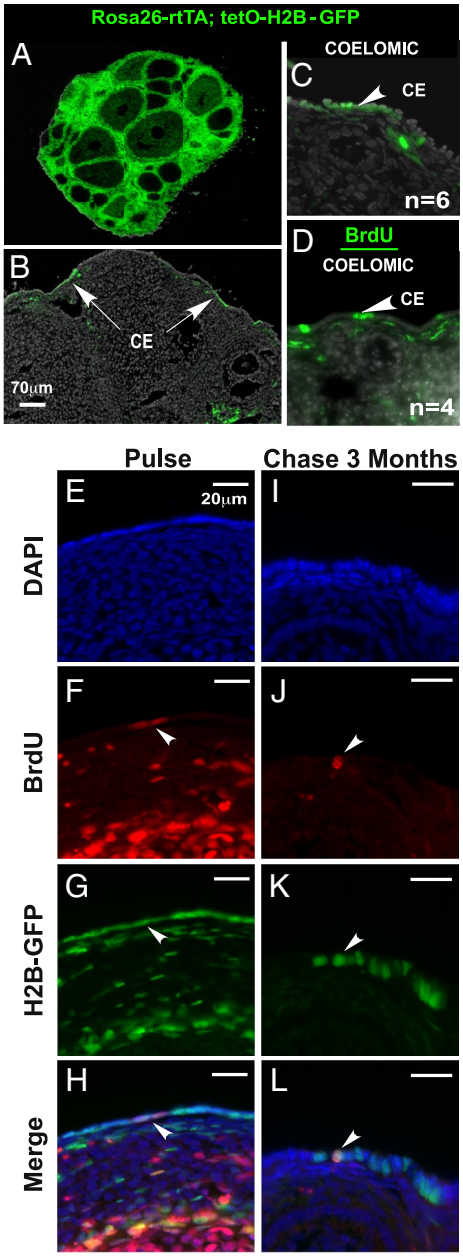

Fig. 1. Identification of BrdU and Rosa26-rtTA; tetO-H2Bj-GFP label retaining cells. (*A*) Adult pulse H2B-GFP ovary after initial pulse. (*B*) Three month chase ovaries demonstrate CE LRCs. (*C*) Digital magnification of H2B-GFP CE LRCs and (*D*) BrdU LRCs (n = number of mice). Combination experiments using BrdU and H2B-GFP at pulse (*E–H*) and 3 months chase (*I–L*) demonstrate occasional colocalization (arrowheads), with H2B-GFP showing a larger number of LRCs, reflecting increased labeling efficiencies.

the differences were less marked (Fig. S3*B*) (adult pulse H2B-GFP = 5.5%, embryonic pulse H2B-GFP = 5.1%, and adult pulse BrdU = 2.2%) after 3 months of chase.

After 3 months chase, gross observation of H2B-GFP ovaries demonstrated epifluorescent LRCs on the surface epithelium (not shown). The three distinct labeling experiments performed in this study identified a consistent population of LRCs (see Fig. 1*B–D*) in the CE. Colocalization of BrdU and H2B-GFP was consistently observed throughout the chase (see Fig. 1 *E–L*).

Phenotypic Characterization of Ovarian LRCs and their Microenvironment. To understand better the identified LRC population, we evaluated a series of known stem, epithelial, mesenchymal, bone

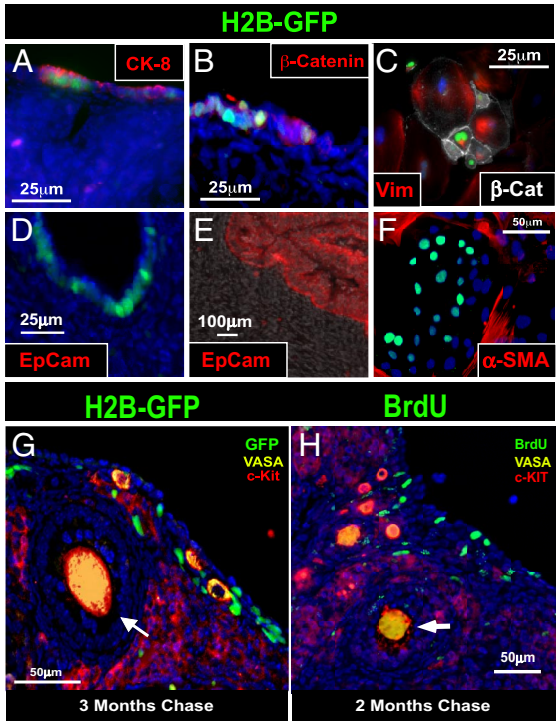

Fig. 2. Phenotypic characterization of ovarian LRCs. After 3 months chase, coelomic LRCs are cytokeratin-8 (*A*), β-catenin (*B* and *C*) and vimentin (*C*) positive. (*D*) Coelomic LRCs are negative for EpCam. (*E*) Normal uterus as a positive control for EpCam. (*F*) Coelomic LRCs are also negative for α-smooth muscle actin. (*G* and *H*) Colocalization of VASA+/c-Kit+ oocytes (arrows) with either H2B-GFP or BrdU at 3 and 2 months chase, respectively, was not observed. Figures representative of $n = 3$.

marrow, germ cell, and ovarian cancer cell markers. Immunofluorescence of H2B-GFP LRCs in tissue and separated CE LRCs *in vitro* demonstrate that these cells express cytokeratin 8 (Fig. 2*A*), β-catenin (Fig. 2 *B* and *C*), vimentin (Fig. 2*C*), E-cadherin, collagen IV, PTEN, gata-4, and PI3K (not shown), and are negative for EpCam (Fig. 2 *D* and *E*), α-smooth muscle actin (Fig. 2*F*), c-kit, CD90, CD45, and CD31 (not shown). Additionally, neither H2B-GFP (Fig. 2*G*) nor BrdU (Fig. 2*H*) LRCs colocalized with VASA+/c-Kit+ germ cells or primordial follicles at any time.

LRCs Replicate in Response to the Estrous Cycle *in Vivo*. To assess the coelmoic LRCs as functional candidate stem/progenitor cells, we explored the capacity of LRCs to proliferate in response to physiologic estrous cycling using stage-specific short-term Iododeoxyuridine (IdU) injections after long term chases. Pre- and postovulatory H2B-GFP 12 week chase mice were timed, stage-confirmed by vaginal cytology, and injected with IdU 2 to 4 h before sacrifice to identify actively mitotic cells. Preovulatory ovaries showed no colocalization of IdU with H2B-GFP CE LRCs (Fig. 3*A*), indicating that before ovulation these LRCs are nonproliferative. Following ovulation, we identified colocalization of IdU with H2B-GFP LRCs in the interfollicular clefts at the edges of the corpus lutea (see Fig. 3 *B* and *C*) and on either side of the repairing epithelium (see Fig. 3 *B* and *D*) indicating that coelomic LRCs are mitotically responsive to the estrous cycle postovulation in these regions.

Coelomic LRCs Show Increased Growth Potential *in Vitro*. A CFU assay was used to detect ovarian CE cells capable of generating colony growth. After 1 to 3 months of chase, H2B-GFP CE cells were released by collagenase treatment and plated. After plating the unsorted population and incubating for 14 days, the average

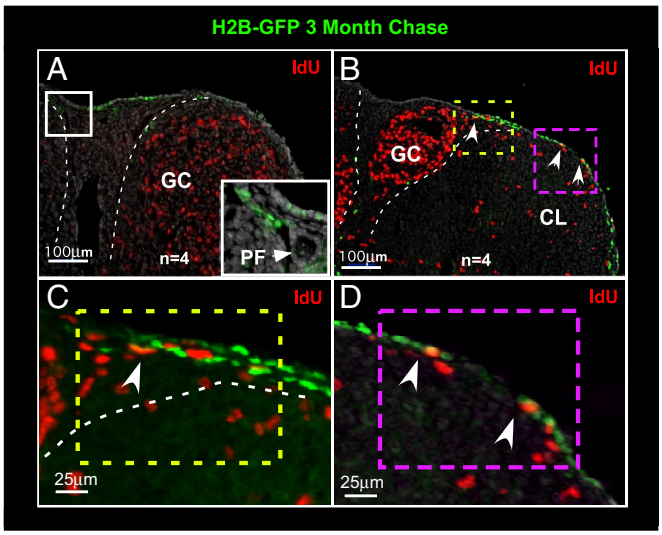

Fig. 3. LRCs replicate in response to the estrous cycle indicating *in vivo* function. (*A*) Preovulatory ovaries demonstrate IdU incorporation in granulosa cells with no colocalization with CE LRCs. (*B*) Postovulatory ovaries demonstrate IdU incorporation into CE LRCs at the edge of the CL and the epithelium overlying the ovulation wound (wound = purple box; CL edge = yellow box). (*C*) CE LRCs were observed to colocalize with IdU (arrowhead) in close association with a maturing follicle. (*D*) CE LRCs were also observed to colocalize with IdU (arrowheads) on either side of the re-epithelializing ovulation wound. Figures representative of $n = 3$. GC = granulosa cells, PF = primordial follicle, CL = corpora lutea.

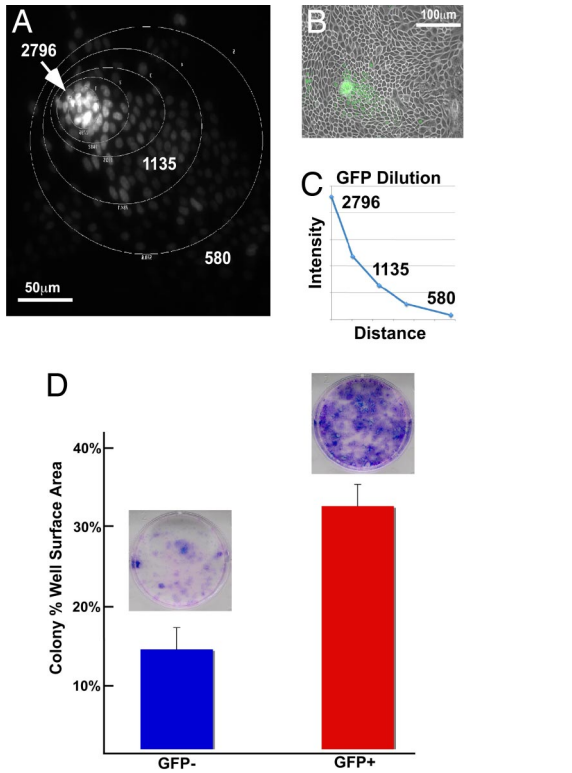

Fig. 4. Coelomic LRCs growth characteristics *in* vitro. (*A*) Identified GFP+ colonies showed a GFP-intense three-dimensional structure (*B*) at the center. (*C*) Intensity quantification showed an exponential loss of signal as a function of the distance from the brightest LRCs. (*D*) H2B-GFP 4 month chase CE cells sorted for GFP show increased colony formation by well surface area percentage compared to non-GFP cells (35% versus 14%, $P < 0.05$, $n = 3$). Representative Giemsa-stained non-GFP and GFP wells (*D Inset*) shown above their respective graph bars.

number of Giemsa-stained colonies observed was 10 ± 5 CFUs per 1×10^4 plated cells ($n = 9$) at each of the chase time-points (not shown).

Confocal microscopy showed that colony-forming H2B-GFP LRCs maintain a three-dimensional structure as their dividing daughter cells proliferate and dilute the H2B-GFP signal (Fig. 4*A*,*B*). Quantification of H2B-GFP signal intensity loss ($n = 3$) with replication was determined to be exponential and a function of distance from the brightest LRC (Fig. 4*C*).

To elucidate further the growth potential of LRCs, CE cells from 4 month chase H2B-GFP mice ($n = 3$) were separated, sorted into GFP+ LRCs and GFP-non-LRCs before being plated in the described CFU assay at a density of 1×10^4 cells per well. Label-retaining GFP cells showed increased growth potential after 14 days as measured by colony formation density when compared to non-GFP cells (35% versus 14%, $P < 0.05$, $n = 3$) (Fig. 4*D*).

SP Enrichs for H2B-GFP LRCs in the Coelomic Epithelium. Chase H2B-GFP ovarian CE cells were isolated by collagenase treatment and subjected to SP analysis (1 month $n = 3$, 2 month $n = 3$, 3 month $n = 1$). We identified a verapamil-sensitive SP within the normal CE in adult H2B-GFP mice (Fig. 5 *A* and *B*). Intensity gates were set using wild type epithelial cells. Evaluation of 2 month chase SP cells for H2B-GFP expression demonstrated that $56.5 \pm 4.1\%$ SD of SP^+ cells are H2B-GFP^+ and that $67.7 \pm 8.1\%$ of these cells are classified as bright LRCs (Fig. 5*C*). Given that less than 15% of the ovary is expected to be GFP or BrdU positive after a 2 month chase (Fig. S3*A*), these findings demonstrate a significant enrichment for LRCs by the SP.

Discussion

By using H2B-GFP and BrdU pulse–chase experiments, we have identified a population of label-retaining ovarian coelomic epithelial cells that are quiescent, slow-cycling, and may undergo asymmetric division (see Fig. 1 *A*–*D*). If all of the cells in the coelomic epithelium contributed equally to postovulation repair, one would expect homogenous dilution of label with wash out after a chase period, as is the case in other tissues (30). Rather, we identify cells that retain label after up to 4 months of chase, indicating that these cells divide much less frequently than the surrounding tissue. This difference in cell turnover suggests that these LRCs have a biologic behavior distinct from their surrounding nonlabel retaining counterparts.

Despite the initial labeling variability between the different H2B-GFP and BrdU experiments, we are confident that the LRCs identified after chase represent the same quiescent population for two reasons. First, the differences in initial labeling among the three pulse schedules did not persist after the chase period. Second, we observed consistent colocalization between the BrdU and H2B-GFP throughout the pulse–chase experiments (see Fig. 1 *E*–*L*). The initial labeling variability likely represents poor Rosa26-rtTA expression in immature granulosa cells, the accepted but shorter labeling period for BrdU (8, 33), and the inability of BrdU to label nondividing cells.

Furthermore, we demonstrate that the identified coelomic LRCs are functionally responsive to estrous cycling *in vivo*. The pattern of IdU incorporation before and after ovulation indicates that the CE LRCs respond to the estrous cycle by replication. The lack of IdU incorporation in the CE LRCs before ovulation (see Fig. 3*A*) demonstrates that these cells are quiescent before ovulation. Localization of the mitotically active LRCs at the interfollicular clefts (see Fig. 3*C*) and at the edge of the epithelial wound (see Fig. 3*D*) after ovulation suggests that the LRCs are involved in the repair and remodeling that necessarily occur after this process and respond to estrous cycling.

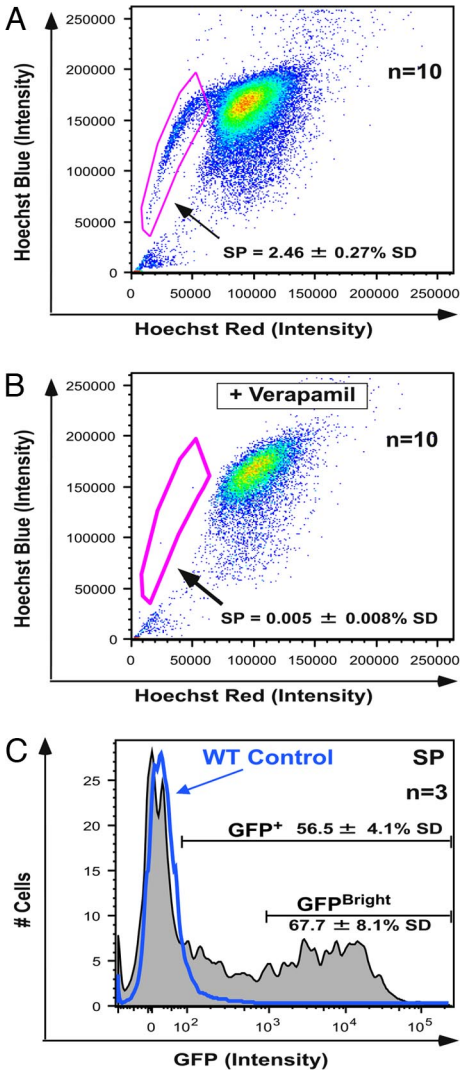

Fig. 5. EeEEnrichment of H2B-GFP LRCs by coelomic epithelial SP cells. (*A* and *B*) The H2B-GFP CE has a verapamil-sensitive SP (2.46 ± 0.27%; $n = 10$). (*C*) Wild type coelomic epithelial cells (blue line) were used to establish a GFP$^+$ intensity gate of $\geq 10^2$ and a GFP^{Bright} intensity gate of $\geq 10^3$. At 2 months chase, 56.5 ± 4.1% of SP cells were GFP$^+$ and 67.7 ± 8.1% of GFP$^+$/SP$^+$ cells were GFP^{Bright}.

The growth characteristics exhibited by the LRCs *in vitro* are consistent with those expected of somatic stem/progenitor cells. Even after disruption of the cellular microenvironment and 14 days of incubation and proliferation *in vitro*, strongly labeled GFP cells can still be identified in a number of colonies (see Fig. 4 *A* and *B*). Additionally, the identified GFP+ colonies exhibit an intensity dilution pattern of exponential signal loss, which is consistent with asymmetric label retention (see Fig. 4*C*). Most convincingly, the H2B-GFP LRCs after 4 months of chase showed significantly more growth and colony formation when compared with nonlabel retaining cells (see Fig. 4*D*). Taken together, the *in vitro* growth characteristics indicate that LRCs have distinct biologic characteristics consistent with somatic stem/progenitor cells.

The side population phenomena of Hoescht 33342 dye efflux has been used to identify a variety of somatic as well as cancer stem cells in various tissues (20–28). The ability to efflux a variety of chemicals is postulated to be a defense mechanism, which leads to the longevity required of somatic stem cells and the chemoresistance characteristic of cancer stem cells (29). We show that the H2B-GFP LRCs comprise 56% of the SP at 2 month chase, representing an almost threefold enrichment of label from the expected 15% or less GFP retention (see Fig. S3*A*) in the whole CE at that point. The majority of LRCs exhibit this chemical-effluxing cytoprotective capacity. The enrichment of LRCs by SP gives one confidence in using the SP as a selection marker for identifying and isolating cell populations that would significantly overlap with the population identified and isolated by H2B-GFP label retention in circumstances where these transgenic models would be unfeasible.

Surface marker analysis demonstrated that although the coelomic LRCs have an epithelial lineage *in vivo* and *in vitro* (cytokeratin-8$^+$, β-catenin$^+$, E-cadherin$^+$), they are also vimentin$^+$ (see Fig. 2 *A*–*C*), which lends support to the dual epithelial/mesenchymal potential ascribed to the ovarian coelomic epithelium (34, 35). Interestingly, whereas ovarian cancer cells express the surface marker EpCam (36, 37), the CE LRCs were negative (see Fig. 2 *D* and *E*). Although we evaluated a wide range of known cellular markers, we were unable to identify a marker signature that uniquely identified the CE LRCs aside from the SP, as described above. More work needs to be done to characterize a cellular marker profile, which would definitively identify the CE LRC population as well as further characterize their niche.

Collectively, our findings identify a candidate putative somatic stem cell population within the mouse ovarian coelomic epithelium that exhibits the properties of quiescence (label retention), functional response to estrous cycling *in vivo* (GFP-IdU colocalization), enhanced growth *in vitro* (colony formation), and cytoprotection (SP).

The notion that cancer is derived from tissue stem cells is over 100 years old, but only recently has this hypothesis been validated (29, 38) and insight provided into the mechanisms by which mutations are accumulated, passed on to differentiating daughter cells, and ultimately lead to tumor progression. Accumulating evidence suggests that somatic stem cells in niche microenvironments may ultimately undergo mutagenic transformation into cancer stem cells (6, 7, 29). Alternatively, aberrant regulatory signals from the niche microenvironment might also lead to tumorigenesis (6, 7, 29). Because many of the same functional properties that define somatic stem cells also define cancer cells, our identification of candidate somatic stem cells in the adult mouse ovary makes it attractive to suggest that these hypotheses might also apply to the generation of ovarian cancer. Elucidation of the elements that lead to malignant transformation will be made more feasible if we have the normal somatic stem cell for comparison.

Our findings indicate that a better understanding of the molecular mechanisms that regulate the identified somatic stem cells within their niche microenvironment is required. Ultimately, it is the comparison of somatic stem cells and their niche to cancer stem cells that may direct the development of treatments targeted toward chemotherapeutic elusive cancer stem cells, particularly in ovarian cancer.

Experimental Procedures

Animal Housing, Estrous Staging and BrdU/IdU Labeling. All protocols involving animal experiments were approved by the Massachusetts General Hospital Institutional Animal Care and Use Committee. Animals were housed, estrous cycle staged, and pulsed with BrdU and IdU (see SI *Experimental Procedures*).

Transgenic Mice and H2Bj-GFP Label and Chase. H2B-GFP mice purchased from Jackson Laboratories (JAX GEMM Strains, Stock Tg(tetO-HIST1H2BJ/GFP)47Efu/J, Stock Number 005104) were crossed with M2-Rosa26-rtTA mice, generously provided by Konrad Hochedlinger (Boston, MA), for near ubiquitous expression of H2B-GFP in the presence of doxycycline (9, 30, 39). To induce expression of H2B-GFP, embryonic mice were fed doxycycline (2 mg/ml, 5% sucrose drinking water) from E0 to P42 or from 6 to 10 weeks of age. At the end of the pulse period, doxycycline withdrawal suppressed H2B-GFP transgene expression. Colocalization of H2B-GFP with known hematopoietic stem cell surface markers (positive) and transgenic mice not receiving doxycycline served as controls for autoflourescence (see ''Quantification of Labeling'' and ''Flow Cytometry'' below). Embryonic pulsed bone marrow and ovaries were

harvested at pulse day 42 (sexually mature, $n = 3$), chase 1 week ($n = 2$), 2 weeks ($n = 2$), 1 month ($n = 3$), 2 months ($n = 3$), 3 months ($n = 4$), and 6 months ($n = 1$), and evaluated for GFP expression. Adult pulsed ovaries were harvested at pulse 1 month ($n = 3$), chase 1 month ($n = 3$), chase 2 months ($n = 3$), chase 3 months ($n = 1$), and 4 months ($n = 3$). In some instances ($n = 3$) mice were injected with BrdU or IdU (Sigma; 1 mg/ml) 2 h before killing to correlate mitotic cells with H2B-GFP LRCs.

Immunofluorescence. Immunofluorescence and BrdU detection was performed as described (28). Primary and secondary antibodies (see SI *Experimental Procedures*) were diluted in 1% BSA /PBS and incubated in a humidified chamber for 1 h. Nuclei were counterstained with 4′6′-diamidino-2-phenylindole (DAPI 1:20,000) Vectashield (Vector Labs) mounting media. Images were captured using a Nikon 80i epifluorescence scope, SPOT RT-KE Camera, and Spot Advance Software (Diagnostic Instruments). Confocal images and time-lapse live cell images were captured on the BD Pathway imaging system using BD Attovision software. To ensure that the signal observed was not autofluorescence, labeling with Alexa-647-anti-GFP antibody was used to confirm colocalization with epifluorescence.

Quantification of Labeling. Quantification of BrdU and H2Bj labeled nuclei was performed either by flow cytometry or by image acquisition (camera settings: Exp. 500ms; Gamma = 0.95; Gain = 4), and analyzed using ImageJ software (National Institutes of Health) with the nucleus counting plugin (see SI *Experimental Procedures*). Quantification of *in vitro* intensity was performed on the BD Pathway imager using BD Attovision software. Cell nuclei were electronically gated as regions of interest. The individual nucleus of greatest intensity was designated as the point from which loss of signal was measured and sequential elliptical rings of equal numbers of cells were established to estimate the loss of signal intensity. Experiments were performed in triplicate.

Flow Cytometry. To validate the ability of the H2B-GFP model to identify stem cells, we analyzed the bone marrow for colocalization with the known hematopoietic stem cell phenotype of Lin^-/c-Kit^+/$Sca\text{-}1^+$ (38, 39) over the course of the chase by flow cytometry (see SI *Experimental Procedures*). H2B-GFP LRC colocalization and enrichment in the Hoechst 33342 excluding SP phenotype was evaluated in the Flow Cytometry Laboratory of the Department of Pathology and the Center for Regenerative Medicine according to their published protocols (25) and as previously described (28). H2B-GFP coelomic epithelial single cell suspensions were generated (see SI *Experimental Procedures*), cells were stained with Hoechst 33342 (5 μg/ml) dye for 90 min at 37°C, washed, and resuspended in PBS containing 2% FCS for analysis of GFP and SP colocalization using the LSRIII flow cytometer (Becton Dickinson). At least 2.5×10^5 events were collected for each analysis and analyzed using FloJo version 8.1.1 software.

Functional Colony Forming Assay and BD Pathway Live Imaging. Coelomic LRCs were isolate by collagenase treatment after a given chase (see SI *Experimental Procedures*), counted, and 2×10^5, 1×10^5, 5×10^4, 2.5×10^4, 1×10^4, and 5×10^3 cells cultured in 2 ml of Murine MesenCult Media (StemCell Technologies) at 37°C, 5% CO_2 for 14 days to obtain an optimal plating number of 1×10^4 for subsequent studies. Plated cells were routinely observed and imaged for GFP expression and colony formation during incubation. For live imaging, cells were incubated and imaged under the BD Pathway live cell confocal imager (Becton Dickinson) using BD Attovision imaging software. Data analysis was performed using ImageJ software. All experiments were performed in triplicate.

Additionally, coelomic epithelial cells were also sorted into GFP and non-GFP populations before plating in the Murine MesenCult Media as above. Colony formation density was measured as a function of culture well surface area percentage. Images of Giemsa stained tissue wells ($n = 3$) were analyzed using the Particle Analysis module of ImageJ software (see SI *Experimental Procedures*).

Statistics. All *p*-values were calculated with the use of two-tailed student's *t* test. Differences with *P*-values less than 0.05 were considered significant.

ACKNOWLEDGMENTS. We thank Dr. David T. MacLaughlin for his help in critically reviewing this manuscript.

1. Bjersing L, Cajander S (1975) Ovulation and the role of the ovarian surface epithelium. *Experientia* 31:605–608.
2. Bukovsky A, Caudle MR, Svetlikova M, Upadhyaya NB (2004) Origin of germ cells and formation of new primary follicles in adult human ovaries. *Reprod Biol Endocrinol* 2:20.
3. Clow OL, Hurst PR, Fleming JS (2002) Changes in the mouse ovarian surface epithelium with age and ovulation number. *Mol Cell Endocrinol* 191:105–111.
4. Tan OL, Fleming JS (2004) Proliferating cell nuclear antigen immunoreactivity in the ovarian surface epithelium of mice of varying ages and total lifetime ovulation number following ovulation. *Biol Reprod* 71:1501–1507.
5. Murdoch WJ, Townsend RS, McDonnel AC (2001) Ovulation-induced DNA damage in ovarian surface epithelial cells of ewes: prospective regulatory mechanisms of repair/survival and apoptosis. *Biol Reprod* 65:1417–1424.
6. Morrison SJ, Spradling AC (2008) Stem cells and niches: mechanisms that promote stem cell maintenance throughout life. *Cell* 132:598–611.
7. Knoblich JA (2008) Mechanisms of asymmetric stem cell division. *Cell* 132:583–597.
8. Blanpain C, Lowry WE, Geoghegan A, Polak L, Fuchs E (2004) Self-renewal, multipotency, and the existence of two cell populations within an epithelial stem cell niche. *Cell* 118:635–648.
9. Tumbar T, *et al.* (2004) Defining the epithelial stem cell niche in skin. *Science* 303:359–363.
10. Welm B, Behbod F, Goodell MA, Rosen JM (2003) Isolation and characterization of functional mammary gland stem cells. *Cell Prolif* 36 *Suppl* 1:17–32.
11. Welm BE, *et al.* (2002) Sca-1(pos) cells in the mouse mammary gland represent an enriched progenitor cell population. *Dev Biol* 245:42–56.
12. Barker N, *et al.* (2007) Identification of stem cells in small intestine and colon by marker gene *Lgr5*. *Nature* 449:1003–1007.
13. Braun KM, Watt FM (2004) Epidermal label-retaining cells: background and recent applications. *J Investig Dermatol Symp Proc* 9:196–201.
14. Kenney NJ, Smith GH, Lawrence E, Barrett JC, Salomon DS (2001) Identification of stem cell units in the terminal end bud and duct of the mouse mammary gland. *J Biomed Biotechnol* 1:133–143.
15. Morris RJ, Potten CS (1994) Slowly cycling (label-retaining) epidermal cells behave like clonogenic stem cells in vitro. *Cell Prolif* 27:279–289.
16. Oliver JA, Maarouf O, Cheema FH, Martens TP, Al-Awqati Q (2004) The renal papilla is a niche for adult kidney stem cells. *J Clin Invest* 114:795–804.
17. Tsujimura A, *et al.* (2002) Proximal location of mouse prostate epithelial stem cells: a model of prostatic homeostasis. *J Cell Biol* 157:1257–1265.
18. Wu WY, Morris RJ (2005) In vivo labeling and analysis of epidermal stem cells. *Methods Mol Biol* 289:73–78.
19. Szotek PP, *et al.* (2007) Adult mouse myometrial label-retaining cells divide in response to gonadotropin stimulation. *Stem Cells* 25:1317–1325.
20. Goodell MA, Brose K, Paradis G, Conner AS, Mulligan RC (1996) Isolation and functional properties of murine hematopoietic stem cells that are replicating in vivo. *J Exp Med* 183:1797–1806.
21. Al-Hajj M, Wicha MS, Benito-Hernandez A, Morrison SJ, Clarke MF (2003) Prospective identification of tumorigenic breast cancer cells. *Proc Natl Acad Sci USA* 100:3983–3988.
22. Bhatt RI, *et al.* (2003) Novel method for the isolation and characterisation of the putative prostatic stem cell. *Cytometry A* 54:89–99.
23. Haraguchi N, *et al.* (2006) Characterization of a side population of cancer cells from human gastrointestinal system. *Stem Cells* 24:506–513.
24. Jonker JW, *et al.* (2005) Contribution of the ABC transporters Bcrp1 and Mdr1a/1b to the side population phenotype in mammary gland and bone marrow of mice. *Stem Cells* 23:1059–1065.
25. Preffer FI, Dombkowski D, Sykes M, Scadden D, Yang YG (2002) Lineage-negative side-population (SP) cells with restricted hematopoietic capacity circulate in normal human adult blood: immunophenotypic and functional characterization. *Stem Cells* 20:417–427.
26. Wulf GG, *et al.* (2001) A leukemic stem cell with intrinsic drug efflux capacity in acute myeloid leukemia. *Blood* 98:1166–1173.
27. Ono M, *et al.* (2007) Side population in human uterine myometrium displays phenotypic and functional characteristics of myometrial stem cells. *Proc Natl Acad Sci USA* 104:18700–187005.
28. Szotek PP, *et al.* (2006) Ovarian cancer side population defines cells with stem cell-like characteristics and Müllerian Inhibiting Substance responsiveness. *Proc Natl Acad Sci USA* 103:11154–11159.
29. Rossi DJ, Jamieson CHM, Weissman IL (2008) Stem cells and the pathways to aging and cancer. *Cell* 12:681–696.
30. Brennand K, Huangfu D, Melton D (2007) All beta cells contribute equally to islet growth and maintenance. *PLoS Biol* 5:e163.
31. Morrison SJ, Uchida N, Weissman IL (1995) The biology of hematopoietic stem cells. *Annu Rev Cell Dev Biol* 11:35–71.
32. Morrison SJ, Weissman IL (1994) The long-term repopulating subset of hematopoietic stem cells is deterministic and isolatable by phenotype. *Immunity* 1:661–673.
33. Braun KM, *et al.* (2003) Manipulation of stem cell proliferation and lineage commitment: visualisation of label-retaining cells in whole mounts of mouse epidermis. *Development* 130:5241–5255.
34. Auersperg N, *et al.* (1999) E-cadherin induces mesenchymal-to-epithelial transition in human ovarian surface epithelium. *Proc Natl Acad Sci USA* 96:6249–6254.
35. Zhan Y, *et al.* (2006) Müllerian Inhibiting Substance regulates its receptor/SMAD signaling and causes mesenchymal transition of the coelomic epithelial cells early in Müllerian duct regression. *Development* 133:2359–2369.
36. Heinzelmann-Schwarz VA, *et al.* (2004) Overexpression of the cell adhesion molecules DDR1, Claudin 3, and Ep-CAM in metaplastic ovarian epithelium and ovarian cancer. *Clin Cancer Res* 10:4427–4436.
37. Kim JH, *et al.* (2003) Identification of epithelial cell adhesion molecule autoantibody in patients with ovarian cancer. *Clin Cancer Res* 9:4782–4791.
38. Reya T, Morrison SJ, Clarke MF, Weissman IL (2001) Stem cells, cancer, and cancer stem cells. *Nature* 414:105–111.
39. Beard C, Hochedlinger K, Plath K, Wutz A, Jaenisch R (2006) Efficient method to generate single-copy transgenic mice by site-specific integration in embryonic stem cells. *Genesis* 44:23–28.